Adsorber heat exchanger using Al-fumarate beads for heat-pump application – a transport study

David Farrusseng, Cécile Daniel, Conor Hamill, Jose Casaban, Terje Didriksen, Richard Blom, Andreas Velte, Gerrit Füldner, Paul Gantenbein, Patrick Persdorf, et al.

Adsorber heat exchanger using Al-fumarate beads for heat-pump application – a transport study

David Farrusseng,*[a] Cécile Daniel,[a] Conor Hamill[b], Jose Casaban,[b], Terje Didriksen,[c] Richard Blom,[c] Andreas Velte,[d] Gerrit Fueldner,[d] Paul Gantenbein,[e] Patrick Persdorf,[e] Xavier Daguenet-Frick[e] and Francis Meunier[f]

Metal-Organic Frameworks (MOFs) thanks to their Type V water adsorption isotherm ("S-Shape") and large water capacity are considered as potential breakthourgh adsorbents for heat-pump applications. In particular Al(OH)-fumarate could enable efficient regeneration at lower temperature than silica-gel which would allow to adress the conversion of waste heat at low temperature such as found in data centers. Despite greater adsorption capacity features, heat and mass transport limitations could jeopardize potential performances of Al(OH)-fumarate. Such heat and mass transports depend on the size of bodies (mm range), their packing and on the pore structures, i.e. macro-mesopore volume and sizes. This paper describes cost-efficient and scalable synthesis and shaping processes of Al(OH)-fumarate beads of various sizes appropriate for use in water Adsorption Heat Pumps (AHP). The objective was to study transport limitations (ie. mass and heat) in practical e beads which meet mechanical stability requirements. Dynamic data at grain scale has been obtained by Large Temperature Jump method while dynamic data at adsorber scale was obtained on a heat exchanger filled with more than 1kg of Al(OH)-fumarate beads. Whereas the binder content has little impact of mass nor heat transfer in this study, we found that Knudsen diffusion in mesopores of the grain may be the main limiting factor at grain scale. At adsorber scale, heat-transfer within the bed packing as well as to the heat exchanger is likely responsible for slow adsorption and desorption kinetics which have been observed for very low temperature of desorption. Finally, dynamic aspects of observed water adsorption isotherm shift with temeprature is discussed in light of reported reversible structure modification upon temperature triggered water adsorption-desorption .

Introduction

Yearly electricity consumption of data centers is estimated to 300 TWh and represents today around 1.5% of worldwide energy consumption. The energy for cooling the supercomputers using cold air accounts for up to ~40% of total datacentre consumption. The Leibniz Supercomputing Centre in Munich, in collaboration with IBM, developed world's first water cooled supercomputer using water Adsorption Heat-Pump (AHP) to convert wasted heat in useful cooling energy for maintaining the temperature of the chips below critical level [1]. The water cooling technology shall allow the system to be built 10 times more compact while consuming 40% less energy than a comparable air-cooled machine. However a techno-economical study of the whole system points out a Return of Investment longer than 8 years which make this current technology poorly economically attractive [2]. The same study concludes that silica-gel adsorbent performs poorly and that "the introduction of high-performance, nanoporous adsorbents for AHP at moderate cost can significantly reduce the overall heat transfer area of the units and provide an overall reduction in capital cost down to a third of the initial heat exchanger price". There is thus a need to reduce production and installation costs while increasing the performance of adsorbents especially at low driving temperature [3].

The potential benefits of Metal-Organic Frameworks (MOF) due to their Type V water adsorption isotherm ("S-Shape") and high water capacity have been highlighted [4-9]. In particular Al(OH)-fumarate has been studied for its high water working capacity and adsorption-desorption cyclability over hundreds of cycles [10-13]. Most interestingly, Al(OH) fumarate shall enable efficient regeneration at lower temperature than silica-gel [14, 15]. A full scale adsorber using Al(OH)-fumarate coating was demonstrated at Fraunhofer ISE [16]. High volume specific cooling power has been obtained at an efficiency that fits the

[a] Univ Lyon, Université Claude Bernard Lyon 1, CNRS, IRCELYON, F-69626, Villeurbanne, France
[b] MOF Technologies, Belfast, UK
[c] SINTEF Industry, Oslo, Norway
[d] Fraunhofer-ISE, Freiburg, Germany
[e] SPF, HSR Univ. of Applied Sciences Rapperswil, Switzerland
[f] MOFapps, Oslo, Norway
*david.farrusseng@ircelyon.univ-lyon1.fr

requirements of datacentre cooling. The same study reports that a pre-treatment step leads to severe corrosion of the heat exchanger. In contrast, the use of grains as adsorbents appears as a cheap solution and shall address the above mentioned cost and corrosion issues [17]. The filling of the adsorber does not require specific treatments of the heat exchanger and is a cheap and well controlled industrial process. A recent study on a small scale adsorber consisting of Al(OH) fumarate/PVA grains shows a high power of 431 W/kg(ads) for a temperature triplet of 60/22/18°C which has not been achieved by other adsorbents so far [17].

A recent study of Kapteijn points out that heat and mass transfer limitations in MOF grains could jeopardise the potential efficiency of MOFs [18]. Their assumption is that mass transfer limitation may occur since pore size of MOFs are about one order of magnitude smaller than for silica-gel. Also strong efficiency penalty could arise from low thermal conductivity (a factor of ten lower than silica-gel) owing their high porosity.

It is well known that mass and heat transfer in porous shaped bodies depends on the dimension of the body, its packing and the porous structure of the grains (porosity, macro-mesopore size, crystallite size,..). At grain scale, the porosity characteristics depend on the synthesis and shaping processes and parameters. Water adsorption and desorption dynamics as function of pellet size and number of grain layers were studied on MOF-801 and MIL-125-NH_2 using Large Temperature Jump method [19,20]. The authors conclude that "the water adsorption on the grains of 0.2–1.8 mm size are shown to occur under a ''grain size insensitive" mode as the adsorption rate is determined by the ratio of the heat transfer area to the adsorbent mass regardless the grain size". These results were obtained on pellets made by compression without binder which cannot offer a sufficient mechanical stability, especially against attrition. In order to meet technical specification, binders shall be introduced in the formulation of the adsorbent in order to prevent the formation of fine particles in the adsorber [21]. To the best of our knowledge, the study of transport limitations for heat-pump application on practical MOF grains produced by cost-efficient and scalable processes has not been reported.

The paper describes efficient and scalable synthesis and shaping processes of Al(OH)-fumarate beads of various sizes appropriate for use in water Adsorption Heat Pumps (AHP). The objective of the paper is to study transport limitations (ie. mass and heat) in practical beads which contain a binder and meet mechanical stability requirements. Transport data at grain scale are obtained by Large Temperature Jump method while dynamic data at adsorber scale was obtained on a demonstrator using kg of Al(OH)-fumarate beads.

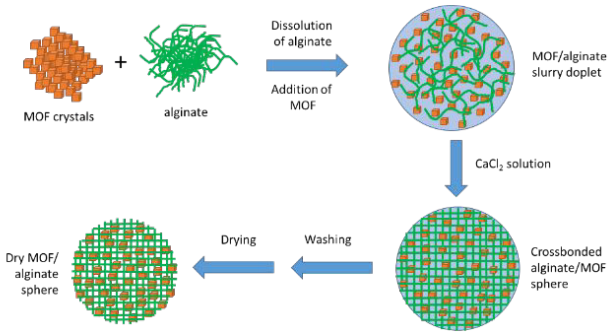

Figure 1: Scheme of MOF bead forming by the alginate dropping process

Experimental

Mechano-chemical synthesis of Al(OH)-fumarate

Al(OH)-fumarate powder was produced on a pilot line using MOF Technologies' patented mechanochemical extrusion process [22]. A recipe similar to that previously reported by Crawford et al. [23] was utilised to synthesise a multi-kg batch of Al(OH)-fumarate. The raw materials $Al_2(SO_4)_3.18H_2O$ (4.39 kg/hr) and $Na_2C_4H_2O_4$ (2.13 kg/hr) were co-fed at stoichiometric ratio into a heated 25 mm co-rotating twin screw extruder at 75°C. The solids reacted to afford Al(OH)-fumarate and a Na_2SO_4 co-product which were axially transported towards a die using a series of screw elements. The product was purified using a water wash, filtered and dried to yield the Al(OH)-fumarate powder.

Bead forming by the alginate dropping process

Granulation by the "alginate" dropping process is a soft chemistry method that has been patented and developed by SINTEF, Oslo (Norway) for controlled MOF-sphere production [24]. Alginate containing water droplets "coagulate" into well-shaped spheres when dropped in a water solution containing a multivalent cation like Ca^{2+}. The metal ion cross-binds the alginate biopolymer into a three-dimensional network with the same size as the droplet. Such 3D spheres are easily separated from the water solution by gravity. The formed beads are dried under ambient conditions for 1 to 3 days. Note that the alginate polymer loses its mechanical properties when heated above 135°C [25].

Series of batches with different bead sizes and binder contents have been prepared at 10g scale in order to study the effect on water uptake and dynamic properties. Two batches of medium (MS) and large (LS) bead sizes have been prepared with the same binder content (22.5wt%). The MS and LS beads of respectively 0.7-1.3 mm and 1.3-1.8 mm have been prepared by

dispensing a Al(OH)-fumarate-alginate suspension (10 g alginate/L) into a 0.2M $CaCl_2$ solution (47.6 g $CaCl_2 \cdot H_2O$/L) through a syringe with appropriate opening diameter. Small sized beads (SS) have been prepared by spraying the Al(OH) fumarate-alginate suspension into a $CaCl_2$ solution using a nozzle combined with an air flow (figure 2). Since the spraying method requires less viscous slurry, an alginate content of 11.8 wt% (dry basis) was used for the SS beads as a compromise between using optimal production conditions but still producing beads with high enough strength. The obtained beads were washed with water and then sieved at three fractions 0.3-0.7mm (SS), 0.7-1.2mm (MS) and 1.3-1.8mm (LS)
In order to study the effect of binder content at identical size, a series of three small sized (SS) beads were prepared at different alginate loading, 11.8, 13.1 and 15.8wt% by spray synthesis as described above, hereafter noted as HL for high loading, ML for medium loading and LL for low loading.
Finally after the study of transport at grain size of the above mentioned samples, a large batch of 1.32kg of small sized beads at low binder content (13.1wt%) was produced by the spray process which was then sieved at 0.3-0.7mm in diameter. This batch was used for measuring the adsorption-desorption dynamic in the adsorber heat exchanger.

Figure 2. Picture of setup used for producing Al(OH)fumarate spheres by spraying the MOF/alginate slurry (to the left) through a nozzle (to the right) by use of a peristatic pump (middle).

Mechanical and ageing characterisation

Crushing strength has been measured on each sphere size fraction by using a Zwick/Roell Z250 universal test machine equipped with 500 N load cell. One bead at a time was placed between the parallel compression plates. The lower compression plate was raised at a rate of 0.2 mm per minute while the force (Newton) was recorded as a function of deformation of the bead in millimeter. The force at the moment when each particle breaks is recorded (TestXpert II) and results for the 3-4 beads are averaged and reported as the average crushing strength.

Attrition tests were conducted to assess the percentage amount of fine particles that the respective beads can generate upon filling the adsorber and maximising the packing by shaking [26]. A 0.2 g mass of material was introduced into a cylinder of 3 cm internal diameter x 2.5 cm height containing an obstacle that the materials hit. This cylinder was made to turn on a classic tube roller (RSLAB-10) at a frequency of 60 rotations per minute (rpm) for 30 minutes. Afterward, the content was passed through a 425 µm sieve to recover fine particles. Attrition percentage is calculated as shown in Equation 1.

$$Attrition = \frac{initial\ mass - recovered\ mass\ above\ 425\ \mu m}{initial\ mass} \times 100$$

Equation 1

Stability upon adsorption and desorption cycles of the beads were evaluated in a home made automated device allowing a fast temperature jump from 30 to 65°C and back (Figure S2). Target temperatures are achieved within 15 s for heating or cooling and keep constant for 2 min before the next cooling/heating step. The open chamber is fed by a continuous flow of humid air at p=24mbar (T_{sat}=20°C). A few beads are placed in an aluminium cup which is posed on the heating/cooling plate. The copper made plate contains a liquid circuit in which hot (up to 75°C) and cold water (down to 20°C) can be fed alternatively from two independent circuits. As a result the relative vapour pressure $(p/p°)_I$ at the sample varies from 10% at 65°C to 57% at 30°C. The stability was assessed by measuring water adsorption isotherms after collecting a few beads at 2000, 6000, 8000 and 10000 cycles, representing in total a duration of about three weeks.

Porosity characterization

Specific surface area S(BET) and micropore volume of the parent Al(OH)-fumarate powders and formed beads were estimated from N_2 isotherms measured at 77K using the BET formalism and t-plot, respectively. The porous structure of beads, i.e. the voids between Al(OH)-fumarate grains and alginate polymer, were analysed by Hg-porosimetry (Micromeritics AutoPore IV 9520) operating from 0.1 Pa to 414 MPa covering the pore diameter range from approximately 360µm to 3nm.

Water adsorption isotherms

Water adsorption isotherms on powder and beads were measured by manometry method using BelSorp MaxII equipment (BelJapan). The purpose of water adsorption measurements is to identify possible degradation or modification of adsorption properties which would have been caused by the shaping process or after ageing. All adsorption isotherms have been measured on typically 200-300mg of beads at 30°C using same equilibrium condition criteria [27]. Because of the degradation of the alginate polymer upon

heating, the samples were evacuated at 30°C prior starting adsorption measurements. Water uptake data are reported to the mass of the dried samples.

Dynamic measurements by Large Temperature Jump (LTJ) method

The LTJ set-up and measurement procedures can be found in earlier studies of authors and in Supporting Information[28,29]. In brief, shaped adsorbent are placed in the measuring chamber on a sample holder, which is attached to the carrier plate of the set-up using thermal grease (Thermigrease TG 20032, Dr. Dietrich Müller Ahlhorn, Germany) in order to achieve a low thermal resistance between sample holder and carrier plate. The temperature of the carrier plate can be changed very rapidly, typically within a second. The surface temperature of the sample is measured with an infrared sensor. For LTJ measurements, the chamber is loaded with water vapour at a certain pressure. The temperature change of the carrier plate will lead to ad- or desorption processes of the sample. Due to the ad- or desorption the pressure in the set-up will change (closed volume). Accordingly, the uptake of the sample can be calculated with the ideal gas law. Adsorption and desorption rates are estimated by the time (s) to achieve 80% of the equilibrium. It was verified that the cumulated adsorption and desorption amount match with equilibrium data measured by isotherms at +/- 10 %. Temperature jump initial and final conditions are the following. For the adsorption jump, the temperature is decreased from 58°C to 35°C which is accompanied with an increase of the relative pressure p/p° from 0.13 to 0.42 (p=23.4mbar). For the desorption jump, the temperature is increased from 51°C to 75°C which is accompanied with an decrease of the relative pressure p/p° from 0.43 to 0.15 (p=56.3 mbar).

For the determination of the heat transfer properties, the measuring chamber is filled with dry nitrogen at a pressure between 10 and 50 mbar. Assuming negligible uptake of N_2 (inert-LTJ), the time-dependent behaviour of the surface temperature of the sample depends only on the heat capacity of the sample and the thermal resistance between sample and carrier plate.
The inert-LTJ measurements were conducted from 60 °C to 30 °C at 12 mbar nitrogen pressure and from 60 °C to 90 °C at 42 mbar, which makes the results comparable to other samples already measured at the Fraunhofer ISE.

Samples with different sized beads were tested in monolayer configuration. In addition, the small sized beads with low binder loading (SS-LL) were tested as a two layer configurations as depicted in Scheme 1 which is a more representative packing in an adsorber-desorber heat exchanger. Table 1 presents the samples and configuration studied. Note: kinetic studies were not carried out on large beads because of the very slow dynamics.

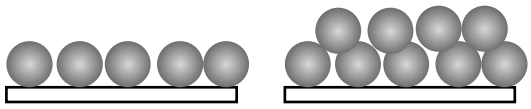

Figure 3: Scheme of layer configuration; mono layer (left), double layer (right)

Table 1: List of LTJ measurements showing amount and area of samples.

Name	Layer config	Bead mass[£] (g)	Adsorbent mass[§] (g)	Area of the sample (cm²)
SS-LL	mono	0.417	0.367	25
SS-LL	double	0.417	0.367	9.61
MS-HL	mono	0.385	0.296	9.61
SS-ML	mono	0.409	0.356	25
SS-HL	mono	0.413	0.348	25

[£] Dry mass of beads with binder (measured), [§]Dry mass of adsorbent without binder (estimated from binder content indicated in Table 2).

Dynamic measurement in an adsorber-desorber heat exchanger

Heat driven cooling machines and heat pumps using solid sorbent material like MOF have a cycling operating principle. This cycling has to be performed due to the limited sorbent capacity of the MOF. While the sorbent is saturated – or partly saturated – by sorbent after an adsorption (half) cycle, a desorption (half) cycle has to follow to regenerate the sorbent. Thus, adsorption and desorption measurements were carried out in a single chamber under sub-atmospheric sorbate vapour pressure conditions (Figure S1). The chamber is designed with a double jacket to avoid any condensation on the chamber walls by temperature condition sustained by a thermostat. For this campaign, 1.32kg of Al(OH)-fumarate beads with bead size of 0.3-0.7mm – corresponding to SS-LL sample material were packed in the Cu tube Al fin adsorber-desorber heat exchanger (hex). The overall hex geometry is length l=400 mm, width w=225 mm, height h=43 mm and a fin pitch of 3mm. A fin thickness of 0.2 mm was used. To keep the granular sorbent in the bed a metal mesh was wrapped around the hex. The total hex mass was 5.18kg. It was suspended at a beam balance which records the mass variation upon adsorption and desorption. Fig S1 shows the open single chamber with the suspended hex and the combined evaporator-condenser underneath. To reach steady state conditions at least 6 adsorption-desorption cycles were carried out. To process the measurement data, prior to sorbate adsorption-desorption a calibration cycling procedures – without sorbate – was made. Adsorption water uptake mass and desorption mass were measured at different time duration (half cycle length tc) of 600s, 750s and 900s. The time tc for adsorption and desorption cycles are always the same. The temperature levels of the heat driven machines adsorption and desorption cycling procedure are determined by the available

external heat sources and heat sinks. As a first approach the temperature conditions during the measurements were defined as follows. During the measurements the temperature conditions were defined as follow. For adsorption step, the temperature of the adsorber was set at 30°C (Tads=30°C) and the temperature of the evaporator at 20°C (Tev=20°C). For the desorption step, the desorption temperature was set at 60°C (Tdes =60°C) and the condensation temperature at 20°C (Tc=20°C).

Results

Characterisation and properties of Al(OH)-fumarate beads

The synthesis yield was higher than 99% and afforded highly porous and crystalline Al(OH)-fumarate. Diffractograms of the MOF produced match those reported in the literature [30]. The surface area is 1098m^2/g (Table 2) which indicates a very high porosity by comparing to other synthesis methods [3]. In contrast to other synthesis methods which use organic solvents (such as DMF) or boiling water, the mechano-chemical extrusion process is solid state and offers significant cost advantages. In addition, the continuous production mode makes the synthesis of high quality Al-fumarate a cost-competitive technology. The shaping process by alginate dropping is also very efficient in the sense that all the MOF containing slurry is converted in beads (no loss of material). It is also a versatile process as the size of the beads can be controlled by the size of droplets (Figures 4, 5 and S6-7). Finally, it is also a scalable process as demonstrated by the production of 1.32kg of small size bead with diameter centred at 0.7µm for this particular study (Figure S4).

While the surface area of the SS beads shows a 10% reduction with respect to S(BET) measurements compared to the starting powder, it is consistent with the amount of binder in the beads (11.8 wt%). The two larger beads (MS and LS) show somewhat lower surface area (-27% and -26% in S(BET), respectively) which are slightly higher than the binder content in these (23.0 and 22.4 wt%, respectively). We can conclude that the alginate binder does not block the micropores of Al(OH)-fumarate.

The cumulative Hg-intrusion curves of the three size bead fraction of Al(OH)-fumarate are shown in Figure S3. The total pore volume is highest for the SS beads (0.94 mL/g) and somewhat lower for the two larger bead fractions (0.75 and 0.81 mL/g respectively). Assuming a crystal density (q) of Al(OH)-fumarate crystal of 1.087 g/cm^3 [31] and assuming that the MOF beads collapse completely at the maximum pressure used in the Hg-porosimetry analyses (414 MPa) and using the total intrusion volumes minus the micropore volumes from N_2 adsorption as estimates of the pore volumes (Vp) of the beads, the total porosity (ε) of the beads can be estimated using the formula $\varepsilon = Vp/(Vp + 1/q)$. Porosities of 0.40, 0.34 and 0.37 are obtained for SS, MS and LS, respectively.

Regarding the size of the voids between crystallites in the beads, the two larger bead size fractions (MS and LS) show typical Hg-intrusion in macropores around 200 nm while the SS fraction exhibit smaller macropores around 60 nm diameter. More importantly, it can be seen that the three bead fractions show a large portion of mesoporous volume with pore diameter below 50nm which could potentially be at the origin of mass transport limitation. The mesoporous volumes comprised between 5nm and 25nm are 0.40, 0.32 and 0.30 cm^3/g for SS, MS and LS beads, respectively.

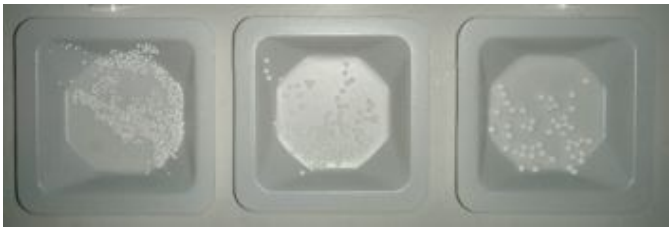

Figure 4: Pictures of the small, medium and large sized beads

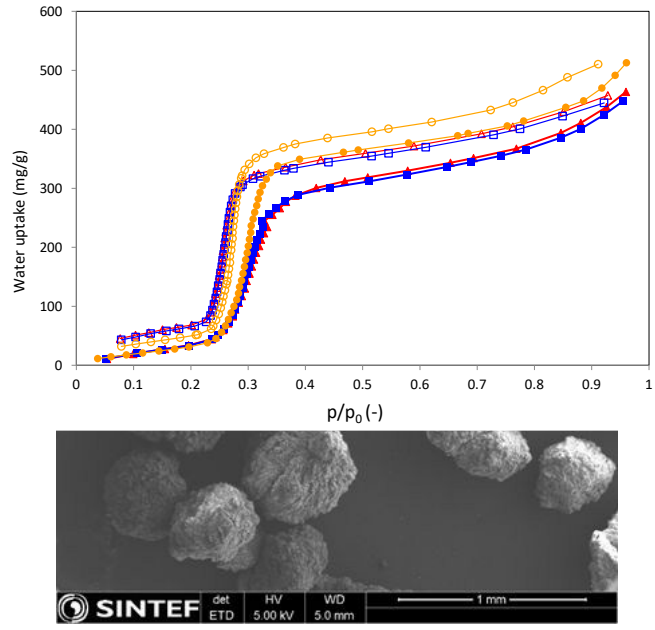

Figure 5: SEM image of small size beads of Al(OH)-fumarate (SS-LL)

Figure 6: Water adsorption isotherms at 30°C of the small (circle), medium (square) and large (triangle) size beads

Direct measurement of the mass and volumes of individually dried beads to estimate the bead densities can only with a reasonable accuracy be done with the two largest size fractions. Bead densities (d) of 0.78 and 0.75 g/cm^3 are obtained as average of 6 individually measured beads with corresponding specific bead volumes of 1.28 and 1.33 cm^3/g for MS and LS size

fractions, specific volume of single crystal Al(OH)fumarate from the crystal density is 0.92 cm^3/g. The difference between the excess specific volumes of the crystal and those estimated for the MS and LS beads are measures of the meso- and macropore volumes as well. The sum of the micropore volume (around 0.30 cm^3/g) and the meso- and macropore volumes estimated this way (0.36 and 0.41 cm^3/g respectively) compare quite well with the total intrusion volumes in the Hg-porosimetry analyses of the MS and LS beads supporting our assumption that Al(OH) fumarate collapses during the Hg-intrusion analyses used when deducing the bead porosities above.

Water adsorption isotherms of the three Al(OH)-fumarate bead fractions show the well-known type V shape and compare very well with published data for Al(OH)-fumarate powder (Figure 6) [30]. It further confirms that the alginate binder does not alter adsorption capacity. As expected the water capacity is penalised by the amount of binder introduced (Table 2). The water adsorption capacities measured at p/p°=0,4 are 0.32, 0.29, 0.28cm^3/g for SS, MS and LS beads respectively which are well in line with micropore volumes estimated by the t-plot method from N_2 physisorption at 77K (0.32, 0.27 and 0.28 cm^3/g for SS, MS and LS, respectively). The effect of binder content can be observed on the desorption branch at low pressure where residual water may be present in the alginate binder (Figure 6 & S5). For all the bead formulation having a large content of binder (MS-HL, LS-HL, SS-LL), the water uptake is approx. 50mg/g at p/p°=0,1 against 35mg/g for lower binder content. Importantly, we can observe significant water uptake for relative pressure (p/p°) above 0.4 which is consistent with the presence of mesoporous volume measured by Hg-intrusion and also the systematic presence of hysteresis between the adsorption and desorption branches in the water adsorption isotherms.

Mechanical and hydrothermal stability of Al(OH)-fumarate beads

The crush strengths are 3.5, 10.2 and 18.0 N for SS, MS and LS, respectively which correlates with the bead diameter. Although the crush strength is low for SS, the strength is high enough to allow easy handling and packing. Equally important is the quasi absence of attrition. The loss of matter after intensive shaking is very low, in the range of measurement limits. We did not observed dust neither which may have slicked on the walls of the rolling cell. The small size beads (SS-LL) were aged over 10.000 cycles of adsorption-desorption in Temperature Swing mode allowing fast swing between adsorption and desorption conditions. Samples were taken after 2000, 6000, 8000 and 10000 cycles. No modifications can be observed in water isotherms.

Kinetic measurements at grain scale using LTJ cell

In Figure 7 the time-dependent behaviour of the surface temperature of different samples is shown for the inert-LTJ measurements under nitrogen atmosphere.

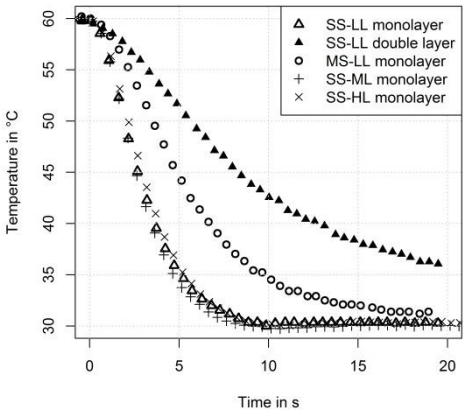

Figure 7: Surface temperature curves for inert-LTJ measurements under nitrogen atmosphere for small and medium bead sizes with mono- our double layer configuration.

We can show that the heat transfer resistance is low for the small beads in monolayer configuration. The heat transfer resistance is slightly higher for medium sized beads in monolayer configuration. We can conclude that the heat conductivity of MOF beads should not be the main source of heat and mass transfer limitations despite the high porosity of the beads. The double layer configuration shows a major heat transfer resistance. It is caused by the additional thermal contact resistance between beads. The binder content has no impact on the heat transfer resistance since the curves for SS-LL, SS-ML, and SS-HL almost match.

In Figure 8 the relative uptake curves for ad- and desorption measurements under water vapour atmosphere are shown. The corresponding values for the calculated water uptake are listed in Table 3. The measured uptake for the samples SS-LL in monolayer and SS-LL in double layer configuration are in good agreement within the measurement uncertainties. According to the equilibrium measurements (isothermal) of Elsayed et al. [15] the loading difference between relative pressures from 0.14 to 0.43 is approximately 0.3 g/g, which is in good agreement with our results. Sample MS-HL shows much lower uptake.

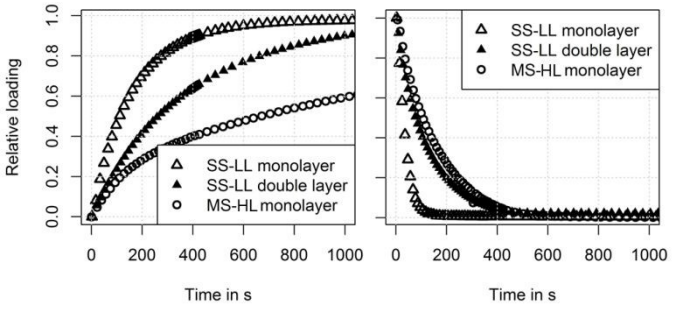

Figure 8: Relative uptake curves for beads of different size and packing in sorption

conditions, Small and medium sized beads (SS-LL and MS-HL) on monolayer configuration and small sized bead (SS-LL) in bilayer configuration.

Table 3: Values for uptake, loading difference for the measurements on monolayer configuration and in double layer configuration in adsorption (ads) or desorption (des) modes after reaching an equilibrium state (3600 s).

Sample	Configuration	Mode	Uptake	Loading difference
			mg	g/g
SS-LL	monolayer	ads	105 +/-5	0.29 +/-0.04
SS-LL	monolayer	des	-106+/-5	-0.29+/-0.04
SS-LL	double layer	ads	125+/-5	0.34+/-0.04
SS-LL	double layer	des	-125+/-5	-0.34+/-0.04
MS-HL	monolayer	ads	65+/-5	0.22+/-0.04
MS-HL	monolayer	des	-65+/-5	-0.22+/-0.04

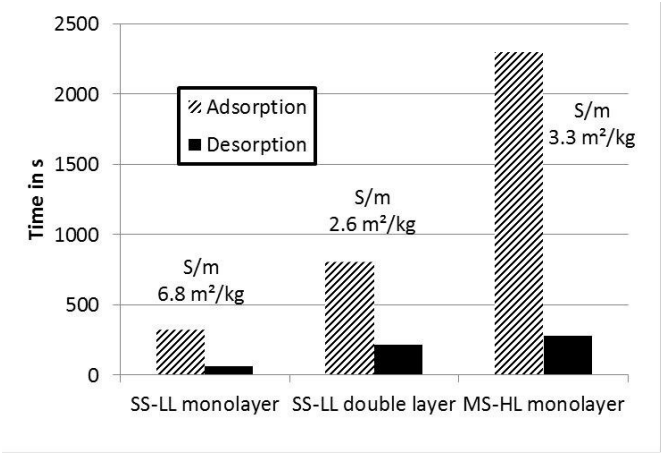

Figure 9: Time to 80% of the equilibrium loading for LTJ measurements under water vapour atmosphere. The ratio S/m is the heat transfer area divided by the adsorbent dry mass of the sample from data in Table 1.

In Figure 9 the time for reaching 80 % of the equilibrium loading difference is shown for the different measurements. It is obvious that desorption is much faster than adsorption for the three investigated samples, although the temperature differences (init-end) are almost the same (23 °C for adsorption, 24 °C for desorption).

The heat transfer surface-adsorbent mass ratio (S/m) is used as indicator of "grain size sensitivity" (Figure 9). Assuming a "grain-size insensitive" mode as proposed by Solovyeva et al. [20] for grain size smaller than 1.8 mm, we would expect faster dynamics for sample MS-HL than SS-LL in double layer configuration. For the SS-LL monolayer and SS-LL double layer the sorption dynamics and the S/m ratios match: The higher the S/m ratio, the faster the dynamics (here: factor 2.5).

However, the adsorption of MS-HL monolayer configuration takes much longer than the adsorption of the SS-LL double layer. Importantly, it is obvious that the size of the beads is a very important parameter which controls transfer processes. Beads with a diameter larger than 0.7 mm show major mass transfer limitation. Here we could assume a main contribution of Knudsen transport regime occurring in the mesopores of the beads. Assuming a hypothetical case where pure Knudsen regime in pores of 10nm would occur with a tortuosity of 2 and a mesoporosity of 50%, the time constant would be in the range of 5.000s for a bead of 1mm of diameter. This hypothetical case could apply for the medium size bead of 0.8-1.2 mm in diameter for which at 1000s only half of the capacity is achieved (Figure 8, MS-HL on adsorption curve).

The hypothesis of a strong mass transfer limitation can also be supported by comparing the dynamics of the adsorption and desorption measurements. The main difference between adsorption and desorption measurements is the higher pressure of water vapour (56.3 mbar vs. 23.4 mbar). All mass transfer processes in macro- or mesopores depend strongly on the pressure of the water vapour [32]. The higher pressure under desorption conditions will speed up the mass transfer processes significantly.

Also the effect of the binder content was studied. The relative uptake curves are shown in Figure 10. For this study only the small size beads were measured. The values for the calculated water uptake are listed in Table 4. These values are in good agreement within the measurement uncertainties and also in good agreement with adsorption equilibrium data.

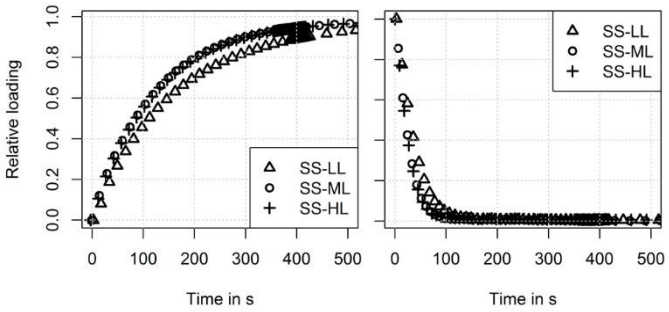

Figure 10: Relative uptake curves for three samples in monolayer configuration with different binder contents. Adsorption (left) and desorption (right).

Table 4: Values for uptake after reaching an equilibrium state (3600 s) for small size beads with different binder contents and layer configurations, loading difference and measurement uncertainties for the measurements of samples SS-LL, SS-ML, and SS-HL

Sample	Configuration	Mode	Uptake in mg	Loading difference in g/g
SS-LL	monolayer	ads	105+/-5	0.29+/-0.04
SS-LL	monolayer	des	-106+/-5	-0.29+/-0.04
SS-ML	monolayer	ads	114+/-5	0.32+/-0.05
SS-ML	monolayer	des	-114+/-5	-0.32+/-0.05
SS-HL	monolayer	ads	114+/-5	0.33+/-0.05
SS-HL	monolayer	des	-115+/-5	-0.33+/-0.05

The kinetics of the adsorber is much slower than the monolayer bead configuration. In the packing of the heat-exchanger, we can estimate that there is a packing 6 to 10 beads (0.3 – 0.7mm; 0.5mm of average diameter, particle size distribution) between the lamellas (separated by 3mm) which does not directly correspond to the two beads configuration of the LTJ cell.

The binder content has a very minor effect on the kinetics of adsorption and desorption. Interestingly, it is found that higher binder contents allow a slightly faster kinetics. However, this difference could come from a slightly larger mean diameter of the beads of the sample with low binder content SS-LL and was not studied further.

Dynamic measurements at adsorber-desorber scale

Water dynamic adsorption as mass uptake as function of time curves are shown for adsorption and desorption in Fig. 11 and Fig. 12, respectively while the cumulated cycled mass are reported in Table 5. Although the temperature conditions in adsorption and desorption at the different cycle tc lengths were not the same the overall shape can be described by an exponential function behaviour. But at the onset of the desorption a time delay of the mass decrease can be observed. The desorption delay time is in the range of 70s for all t_c. While in adsorption, the curves for all t_c, the kinetics shows the same behaviour and the data are within the experimental measurement uncertainty, the desorption behaviour is different. This asymmetry can be assigned to the dominant driving forces, namely adsorption pressure and desorption temperature (no independent control of the forces: temperature T & sorbate pressure p) and to the heat-exchanger characteristics. In the adsorption step, the water vapour flows towards an open heat exchanger surface of granular Al(OH)-fumarate fixed bed - the adsorption process and thus the mass increase starts immediately. In the desorption step, the vapour has to flow in the opposite direction. But to do so, the total mass has to be heated up and due to the thermal mass the mass desorption underlies a time delay.

Table 5: Cumulated water adsorption or desorption in cycling conditions considering different cycle lengths.

Cycle time (s)	mass in adsorption (g)	mass in desorption (g)
600	100.7 +/-8	103.0 +/-8
750	124.9 +/-8	138.0 +/-8
900	144.3 +/-8	166.8 +/-8

Figure 11: Adsorption dynamics of water on the full scale adsorber-desorber heat and mass exchanger at different half cycle lengths of 600s, 750s and 900s. (The y-scale is in g for the 1.32kg Al-Fumarate)

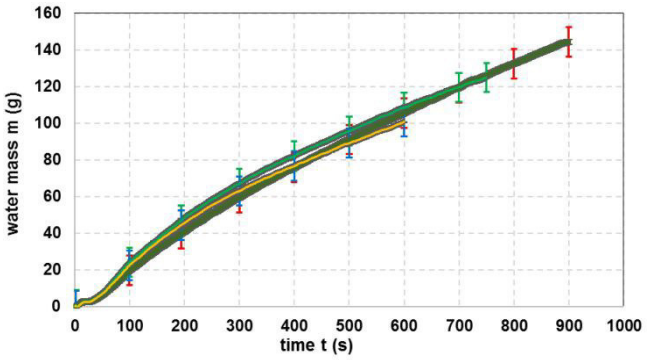

Figure 12: Adsorption dynamics of water on the full scale adsorber-desorber heat and mass exchanger at different half cycle lengths of 600s, 750s and 900s. (The y-scale is in g for the 1.32kg Al-Fumarate)

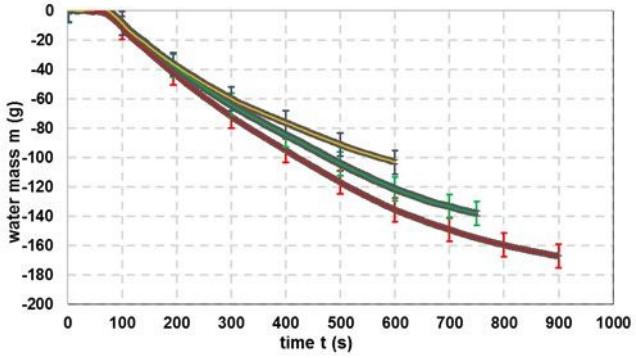

Discussion

In addition to a "S" type water adsorption isotherm Al(OH)-fumarate, there is a "shift" of the isotherm in relative humidity (p/p°) when the temperature increases. Whereas the inflexion point of the isotherm (alpha value) is at p/p°=0,27 at 30°C, and at p/p°=0,32 at 55°C (S8) [33]. This peculiar phenomena has been observed earlier and more recently confirmed on samples prepared by very different synthetic methods[11,34]. On the other hand, reversible structural modifications of Al(OH)-fumarate

upon water adsorption-desorption by heating have been observed by powder X-Ray Diffraction[11]. As Al(OH)-fumarate is a structural analogue of Al-MIL-53 which structures is sensitive to guest inclusion in a cooperative mode, the authors assumed that the reversible structure modification upon heating in humid chamber is likely due to the presence/absence of water guest molecules in the pores. Pushing the assumption further, this structural transformation upon heating could be at the origin of the major water isotherm "shift" in relative pressure as indicated above. Indeed, adsorption isotherms and in situ XRD have been measured at thermodynamic equilibrium of the adsorption process. On heat-transformation process point of view, such an isotherm "shift" when the temperature increases would be beneficial as it means that the adsorbent can be regenerated at higher relative humidity than expected according to isotherms recorded at lower temperature. This gain in regenerability would be of great value in the frame of low temperature driving application such as data centre cooling. However, it is not obvious whether this structural transformation occurs and could be completed in limited time corresponding to adsorption or desorption process cycles. In this study, we have shown that at grain scale the uptake/desorption can be completed within 1-10 minutes depending on the size of the grain. The question which is now open is whether the structure transformation (i.e. cooperative phenomenon) is faster or slower than the observed mass transport and therefore can be actually an asset for cooling applications.

Conclusions

Compared to other recent studies on transport of MOF grains, our study deals with MOF beads which have been produced by efficient and scalable processes. We have shown that alginate dropping process yields shaped beads with required mechanical and hydrothermal stability. In particular, the alginate binder prevents attrition upon shaking which is a prerequisite when filling a heat exchanger by shaking. Although the binder content reduces the water working capacity equally to its content, rising binder content does neither modify the shape of the adsorption-desorption isotherms nor induce additional mass transfer resistance. From LTJ inert measurements, we conclude that heat transfer resistances are smaller than mass transfer resistances for the studied Al(OH)-fumarate beads and thus to not limit adsorption dynamics in this case.

This study reveals the importance of the porous structure of the beads which are barely studied. In particular, we show the presence of large amount of mesoporous volume, especially small mesopores with pore diameter below 20nm. We can assume that major mass transfer resistance may be due to Knudsen regime at grain scale. This assumption is supported by the findings that the bead size has a very strong impact of dynamic uptake. Whereas the small size beads show relatively fast kinetics, the medium size beads show slow kinetics and we could not measure the dynamics of the largest bead fraction as the phenomenon was too slow. This study points out the importance played by the pore structure at the scale of the grain. Ideally, the shaping process should limit to large mesopores especially when beads of 1mm in diameter or above would be preferred for industrial applications.

This study also reports the dynamic measurements in cycling mode of an adsorber-desorber consisting in a heat-exchanger filled with 1.32kg of Al-(OH)-fumarate beads of 0.7mm diameter. The equilibrium was not achieved after 900s at very soft desorption conditions however (T desorption =60°C - T condensation =20°C). The slow kinetics observed in the adsorber may arise from the poor heat transfer of the bead packing as observed for double layer configuration and/or the heat exchanger design.

Whereas cooperative phenomena in adsorption-desorption are now well established in flexible porous solids, dynamic aspects of the same phenomena have not been addressed at the same level yet. As highlighted here, conclusions will not be straightforward as there is an interplay with mass and heat transfer at different scales.

Conflicts of interest

There are no conflicts to declare

Acknowledgements

This work has been carried out within the ProDIA project that has received funding from the European Union's Horizon 2020 research and innovation programme under grant agreement No. 685727

We would like to acknowledge the work of Maximilian Baumgarten who prepared the samples at Fraunhofer ISE, conducted the LTJ and inert-LTJ measurements, and evaluated the inert-LTJ measurements for his Bachelor thesis.

Notes and references

‡ Supporting information available.

1. T. Wilde, M. Ott, A. Auweter, I. Meijer, P. Ruch, M. Hilger, S. Kühnert and H. Huber, 2017.
2. M. Ott, T. Wilde and H. Huber, Orlando, FL, USA 2017.
3. E. Hastuerk, S-B. Ernst and C. Janiak, Current Opinion in Chemical Engineering, 2019, **24**, 26-36
4. Y. Aristov, *Applied Thermal Engineering*, 2014, **72**, 166-175.
5. M. Erdos, M. F. de lange, F. Kapteijn, O. A. Mouttos and T. J.

H. Vlugt, *Acs Applied Materials & Interfaces*, 2018, **10**, 27074-27087.
6. M. F. de Lange, K. J. F. M. Verouden, T. J. H. Vlugt, J. Gascon and F. Kapteijn, *Chemical Reviews*, 2015, **115**, 12205-12250.
7. F. Jeremias, D. Froehlich, C. Janiak and S. K. Henninger, *New Journal of Chemistry*, 2014, **38**, 1846-1852.
8. J. Canivet, A. Fateeva, Y. Guo, B. Coasne and D. Farrusseng, *Chemical Society Reviews*, 2014, **43**, 5594-5617.
9. P. G. M. Mileo, K. Ho Cho, J. Park, S. Devautour-Vinot, J.-S. Chang and G. Maurin, *J. Phys. Chem. C*, 2019, **123**, 23014-23025.
10. S. Kayal, A. Chakraborty, HWB Teo, *Materials Letters*, 2018, **221**, 165-167
11. F. Jeremias, D. Froehlich, C. Janiak, SK. Henninger, *RSC Advances*, 2014, **4**(46), 24073-24082
12. H.W.B, Teo, A. Chakraborty, Y. Kitagawa, S. Kayal, International Journal of Heat and Mass Transfer, 2017, **114**, 621-626
13. H.W.B, Teo, A. Chakraborty, S. Kayal, Microporous Mesoporous Mat., 2018, 272, 109-116
14. F. Meunier, *Science*, 2017, **358**, eaao0361.
15. E. Elsayed, R. Al-Dadah, S. Mahmoud, P. Anderson and A. Elsayed, *Desalination*, 2020, **475**.
16. H. Kummer, F. Felix Jeremias, A. Warlo, G. Füldner, D. Fröhlich, C. Janiak, R. Gläser and S. K. Henninger, *Ind. Eng. Chem. Res.*, 2017, **56**, 8393−8398.
17. S. Goekpinar, S.-J. Ernst, E. Hastuerk, M. Moellers, I. El Aita, R. Wiedey, N. Tannert, S. Niessing, S. Abdpour, A. Schmitz, J. Quodbach, G. Fueldner, S. K. Henninger and C. Janiak, *Industrial & Engineering Chemistry Research*, 2019, **58**, 21493-21503.
18. S. Graf, F. Redder, U. Bau, M. de Lange, F. Kapteijn and A. Bardow, *Energy Technol*, 2019, 1900617-.
19. M. V. Solovyeva, Y. I. Aristova and L. G. Gordeeva, *Applied Thermal Engineering*, 2017, **116**, 541-548.
20. M. V. Solovyeva, L. G. Gordeeva, T. A. Krieger and Y. I. Aristova, *Energy Conversion and Management*, 2018, **174**, 356-363.
21. S. Hindocha and S. Poulston, *Faraday Discussions*, 2017, **201**, 113-125.
22. Patent WO2014191725.
23. D. Crawford, J. Casaban, R. Haydon, N. Giri, T. McNally and S. L. James, *Chemical Science*, 2015, **6**, 1645-1649.
24. A. I. Spjelkavik, A. Swapnil Divekar, T. Didriksen and R. Blom, *Chem., Eur. J.*, 2014, **20**, 8973-8978.
25. D. W. Lee, T. Didriksen, U. Olsbye, R. Blom and C. A. Grande, *Sep. Purif. Techn.*, 2020, **235**, 116182
26. Y. Khabzina, J. Dhainaut, M. Ahlhelm, H.-J. Richter, H. Reinsch, N. Stock and D. Farrusseng, *Ind. Eng. Chem. Res.* , 2018, **57**, 8200-8208.
27. J. Canivet, J. Bonnefoy, C. Daniel, A. Legrand, B. Coasne and D. Farrusseng, *New Journal of Chemistry*, 2014, **38**, 3102-3111.
28. A. Velte, G. Fueldner, E. Laurenz and L. Schnabel, *Energies*, 2017, **10**, 1130.
29. A. Sapienza, A. Velte, I. Girnik, A. Frazzica, G. Füldner, L. Schnabel and Y. Aristov, *Renewable Energy*, 2017, **110(C)**, 40-46.
30. N. Tannert, C. Jansen, S. Niessing, C. Janiak, *Dalton Trans*. 2019, **48**, 2967
31. E. Elsayed, R. Al-Dadah, S. Mahmoud, P. A. Anderson, A. Elsayed and P. G. Youssef, *Desalination*, 2017, **406**, 25-36.
32. W. Kasta and C.-R. Hohenthanner, International Journal of Heat and Mass Transfer, 2000, **43**, 807-823.
33. J. Canivet, J. Bonnefoy, C. Daniel, A. Legrand, B. Coasne, D. Farrusseng, *New J. Chem*, 2014, **38**, 3102–3111.
34. N. Hanikel, M. S. Prévot, F. Fathieuh, E.A. Kapustin, H. Lyu, H/ Wang, N. J. Diercks, T. Grant Glover, O. Yaghi, *ACS Cent. Sci*. 2019, **5**, 1699−1706

Table 2: Sample composition, porous structures and mechanical characteristics

Samples	Code	Diameter	Binder content	Surface area[§]	Micro-pore volume[§]	Pore volume[§]	Water uptake at p/p°=0,4[$]	Macro-mesopore volume[¤]	Bead density*	Crushing strength	Loss by attrition
		mm	wt%	m^2/g	cm^3/g	cm^3/g	cm^3/g	cm^3/g	$g.cm^{-3}$	N	%
Powder	Powder	n.a.	n.a.	1098	0.36	n.a.	n.a	n.a.	n.a.	n.a.	n.a.
Small Size-Low Loading	SS-LL	0.3-0.7	11.8	997	0.32	0.96	0.35	0.62	-	3.5	0,5
Medium Size-Low Loading	MS-HL	0.7-1.2	23	801	0.27	0.53	0.29	0.48	0.78	10.2	0.6
Large Size-High Loading	LS-HL	1.3-1.8	22.4	816	0.28	0.55	0.29	0.53	0.75	18.0	0,6
Small Size-Medium Loading	SS-ML	0.3-0.7	13.1	925	0.32	0.67	0.31	-	-	-	0,3
Small Size-High Loading	SS-HL	0.3-0.7	15,8	921	0.32	0.53	0.31	-	-	-	0,3

[§] estimated by S(BET) from N_2 physisorption at 77K, [$] from water isotherm at 30°C, [¤] Macro-mesopore volume estimated from Hg intrusion assuming full collapse of Al-(OH)fumarate crystal structure during the analysis, * from direct measurements of mass and volume on dried beads, n.a. not applicable